Segmental dynamics and incompatibility in hard/soft polymer blends

K. Karatasos, G. Vlachos, D. Vlassopoulos, and G. Fytas
Foundation for Research and Technology—Hellas, Institute of Electronic Structure and Laser, P.O. Box 1527, 71110 Heraklion, Crete, Greece

G. Meier and A. Du Chesne
Max-Planck Institut für Polymerforschung, Box 3148, 55021 Mainz, Germany

(Received 11 November 1997; accepted 5 January 1998)

We report on the segmental dynamics of the binary polymer blend polystyrene (PS)/poly (methylphenylsiloxane) (PMPS) in the two-phase region using dielectric spectroscopy that essentially probes the PMPS component. Based on the experimental orientation relaxation functions, the average glass transition temperature T_g controls phase separation. When the spinodal temperature T_s exceeds T_g, the PMPS segmental relaxation displays two distinct decays characteristic of a merely pure and a mixed, roughly at the initial composition, PMPS regions. On the contrary, when T_s falls in the proximity of T_g, the PMPS relaxation is strongly nonexponential and its average time reflects mixed regions rich in PMPS due to incomplete phase separation, which drives only the glassy phase out of local thermodynamic equilibrium. Distinct morphological differences in the two-phase state of these blends, inferred from their segmental dynamics, are revealed by transmission electron microscopy. © *1998 American Institute of Physics.* [S0021-9606(98)50214-0]

I. INTRODUCTION

The effects of composition fluctuations on the segmental dynamics are known to be crucial in understanding the local dynamics of mixed polymeric glasses. For example, in the case of binary blends and diblock copolymers, several investigations have addressed aspects of this problem.[1–7] Further, an increasing number of experimental studies, as well as theoretical and computer simulation efforts,[8–12] have elucidated the role of the mobility contrast between the components of a binary mixture on, and its relation to, the local immiscibility, clearly observed even in athermal systems.[4,6,7] Recent elaborate experimental studies have demonstrated the effect of the suppression of the composition fluctuations[13–15] which can lead even to the dynamic arrest of phase separation[13] due to vitrification, when the glass transition temperature, T_g, is reached before phase separation occurs at the spinodal temperature, T_s. In contrast to small molecule mixtures, it is the interplay between the local mobility and the thermodynamic driving force, that apparently controls the demixing process and finally determines the morphology of the two phase-region.

In the case where the phase separation process has been completed, resulting in an equilibrium thermodynamic state, an A/B blend's partitioning in *A-rich* and *B-rich* phase is expected to obey the lever rule, with local compositions according to the phase envelope of the binary mixture. Such a system is characterized by the existence of two glass transitions,[16] and two dynamically distinct regimes, modified from the corresponding homopolymer characteristics, by amounts reflecting the average equilibrium compositions in the two phases. On the other hand, when glass transition interferes with the demixing process, the resulting incomplete phase separation will lead to thermodynamically non-equilibrium final stages.[10,13,17] In the latter case, the compositions of the two phases are expected to be different from their nominal values based on the phase diagram. Depending on the degree of demixing, two, or even a single but broad glass transition might be observed,[1,13] rendering thus any conclusion concerning the composition of the two phases rather ambiguous. However, in both cases, information on the degree of evolution of the phase separation can be provided by probing the component's segmental dynamics, reflecting the composition characteristics of the formed local environments. In this context we have performed a detailed dynamic and morphological investigation of phase separated binary polymer blends, with large T_g contrast between components, and the effects of the relative distance between the T_g of the formed phases and the mixture's phase separation temperature on the resulting two-phase state of the mixtures. We have shown that real space morphology can be manifested in the local segmental dynamics of the heterogeneous polymer blends.

II. EXPERIMENT

A. Materials

Polystyrene (PS) and poly(methylphenylsiloxane) (PMPS) samples were synthesized via anionic polymerization. Their molecular characteristics together with the glass transition temperatures measured by differential scanning calorimetry (DSC) are listed in Table I. Five binary polymer blends PS/PMPS were prepared from ternary solutions in a common good solvent, toluene. The solvent was subsequently allowed to evaporate under vacuum at 140 °C for more than a week. The PS volume fraction ϕ in the five binary polymer mixtures and the computed T_g $[1/T_g(\phi) = \phi/T_{g,\mathrm{PS}} + (1-\phi)/T_{g,\mathrm{PMPS}}]$ in the homogeneous state are

TABLE I. Molecular characteristics of the PS and PMPS homopolymers.

$M_{w,\mathrm{PS}}$	M_w/M_n	N_{PS}	$T_{g,\mathrm{PS}}$(K)	$M_{w,\mathrm{PMPS}}$	M_w/M_n	N_{PMPS}	$T_{g,\mathrm{PMPS}}$(K)
3250	1.05	31	356	2720	1.1	20	234
4200	1.05	40	361	6970	1.1	51	239
7600	1.05	73	363	4800	1.1	31	238

listed in Table II. The spinodal temperatures T_s of the blends, shown in Table II, correspond to the temperature at which the light scattering intensity due to composition fluctuations diverges, according to the mean-field theory.

B. Experimental techniques

1. Differential scanning calorimetry (DSC)

The glass transition temperatures of the PS and PMPS homopolymers, as well as the blends, were measured with a differential scanning calorimeter (Rheometric Scientific, model PL-DSC). All blends were brought to the two-phase state, after they had been annealed at 130 °C for several weeks in vacuum followed by slow temperature decrease to ambient temperature in a couple of days. Then the samples were quenched to liquid nitrogen temperature and the DSC traces were measured with a heating rate of 20 K/min. Two representative thermograms from blends A_1 and B are shown in Fig. 1. Two glass transitions were observed in both blends, in consistency with the existence of two different environments in the phase-separated regimes; however, the T_g steps for blend B are hardly seen in accordance with the assumption that no clear phase-separated region is present. Dynamic and morphological data (see Sec. III) will provide information on the phase state of the present blends.

2. Transmission electron microscopy (TEM)

We performed TEM experiments, in order to acquire a direct visualization of the particular morphological characteristics of the blends. Representative images from the two groups of blends were taken, and in particular for blends B ($T_s \approx T_g$) and A ($T_s > T_g$). Ultrathin sections of bulk samples of the blends were produced at -50 °C using a Leica Ultracut UCT with EMFCS cryo-attachment. The sections were floated off the diamond knife on a H_2O–DMSO mixture (40:60) and transferred to the grids. The specimens were left unstained. Electron microscopy was done in a Leo 921-Ω operated at 120 kV. As expected, conventional and elastically filtering brightfield techniques do not reveal contrast strong enough to elucidate any structure. Micrographs were therefore taken in the inelastic imaging mode under the conditions for structure sensitive contrast ($\Delta E = 250$ eV). In the images, regions enriched with PMPS appear brighter than those containing more PS. Details on the method in general and on other siloxane containing polymer systems have been published elsewhere.[18]

3. Dielectric relaxation spectroscopy (DS)

The measurements were performed utilizing a Solartron-Schlumberger FRA 1260 frequency analyzer supplemented by using a high impedance preamplifier of variable gain, in the frequency range of 10^{-2}–10^6 Hz. The sample was kept between two gold-plated stainless steel electrodes (diameter 40 mm) with a spacing of 0.1 mm. The sample cell was placed in a cryostat with its temperature regulated by a nitrogen gas jet heating system, allowing a stability of 0.1 °C and providing control in a broad temperature range (-160–300 °C). All samples were measured either starting from temperatures lower than $T_{g,\mathrm{PMPS}}$, up to the homogeneous phase higher than the $T_{g,\mathrm{PS}}$, or vice versa. The samples used for DS measurements were thermally treated like those for DSC investigations. However, instead of quenching to low temperatures, they were first heated up to 150 °C and where then cooled down with rate of 5 K/min to temperatures well below the T_g of the PMPS. Variation of this cyclus with respect to cooling rates gave identical results with regard to the dielectric response.

C. Data analysis

DS has been shown to be very sensitive in probing local dynamics in multiconstituent polymeric systems,[3,9,19] providing detailed information on a segmental level. The dielectric characteristics of the examined system are associated to its relaxational behavior, by the interconnection[20] of the complex dielectric permittivity, $\epsilon^* = \epsilon' - i\epsilon''$, with the response function $\Phi(t)$. Namely ϵ^* is expressed by the one sided Fourier transform of the time derivative of Φ,

$$\epsilon^*(\omega) - \epsilon_\infty = \Delta\epsilon \int_0^\infty \left(-\frac{d\Phi}{dt} \right) e^{-i\omega t} dt, \tag{1}$$

where $i^2 = -1$, $\Delta\epsilon = \epsilon_0 - \epsilon_\infty$ is the relaxation strength, with ϵ_0 and ϵ_∞ being the low and high frequency limits of ϵ'. In

TABLE II. Characteristics of the various PS/PMPS blends.

PS/PMPS	N_{PS}	N_{PMPS}	ϕ	T_s(K)	ϕ_s	T_g(K)
A	73	20	0.50	383	0.34	285
A1	31	31	0.30	400	0.50	264
A2	73	20	0.75	358	0.34	319
B	31	51	0.45	314	0.56	281
B1	40	20	0.28	317	0.41	260

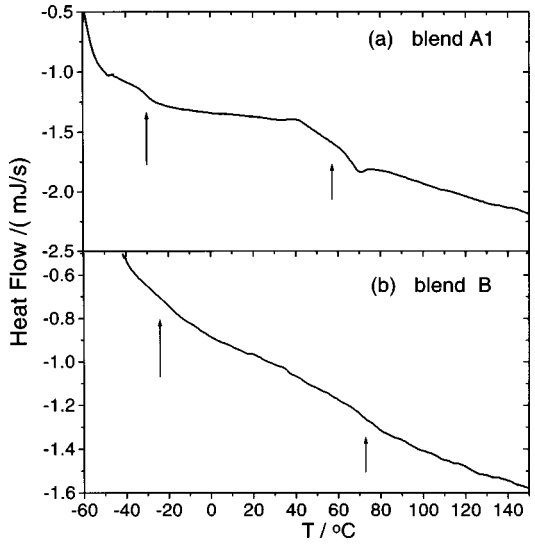

FIG. 1. Differential scanning calorimetry of blends A1 (a) and B (b), indicating two glass transition temperatures (arrows); for blend B the transitions are nearly smeared out, as discussed in the text.

the case of segmental relaxation, in general $\Phi(t)$ represents the normalized autocorrelation function of the segmental dipoles,

$$\Phi(t)=\sum_{ij}\langle\mu_i(t)\mu_j(0)\rangle \Big/ \sum_{ij}\langle\mu_i(0)\mu_j(0)\rangle, \tag{2}$$

where $\mu_i(t)$ is the dipole moment of the ith segment at time t, and $\langle\rangle$ denotes an ensemble average. The cross correlation terms between different segments, cancel out when no association or specific interactions are present, hence what is measured, is the normalized self-correlation function of the segmental dipole moment reorientation. The strength $\Delta\epsilon$ associated with the dielectric segmental mode relaxation of the species i is expressed by[20]

$$\Delta\epsilon_i=N_A\mu_i^2\rho F/3m_i k_B T, \tag{3}$$

where m_i refers to the segmental mass, μ_i is the backbone dipole moment component perpendicular to the chain (assigned to each segment i), ρ the density, and F the local field factor.[20] Data analysis was performed (i) by means of the well-known Havriliak–Negami[21] (HN) empirical function

$$\epsilon^*(\omega)=\epsilon_\infty+(\epsilon_0-\epsilon_\infty)/[1+(i\omega\tau_0)^\alpha]^\beta, \tag{4}$$

where α and β (α, $\beta\geqslant 0$, and $\alpha\beta<1$) are parameters describing the broadening and the skewness of the relaxation spectrum, respectively; and (ii) by utilization of a new technique for the inversion of frequency domain dielectric data,[22] yielding the distribution of relaxation times and further, more easily the relaxation strength $\Delta\epsilon$, a quantity which is essential to know for our purpose. In the latter method, the dielectric loss spectra are expressed as a superposition of Debye processes on a logarithmic time scale via

$$\epsilon''(\omega)=\int_0^\infty \widetilde{F}(\ln\tau)\omega\tau/[1+(\omega\tau)^2]d\ln\tau, \tag{5}$$

where $\widetilde{F}(\ln\tau)=\Delta\epsilon F(\ln\tau)$; integration of the resulting $\widetilde{F}(\ln\tau)$ yields $\Delta\epsilon$ since the $F(\ln\tau)$ of Debye times is normalized; a similar equation to (5) is also used extensively in the analysis of dynamic mechanical data. The characteristic relaxation time can be extracted from the peak position of the distribution. Besides the loss due to relaxation, an additional contribution to the spectra may arise from ionic conductivity, $\epsilon''\propto\omega^{-1}$, only apparent at low frequencies.

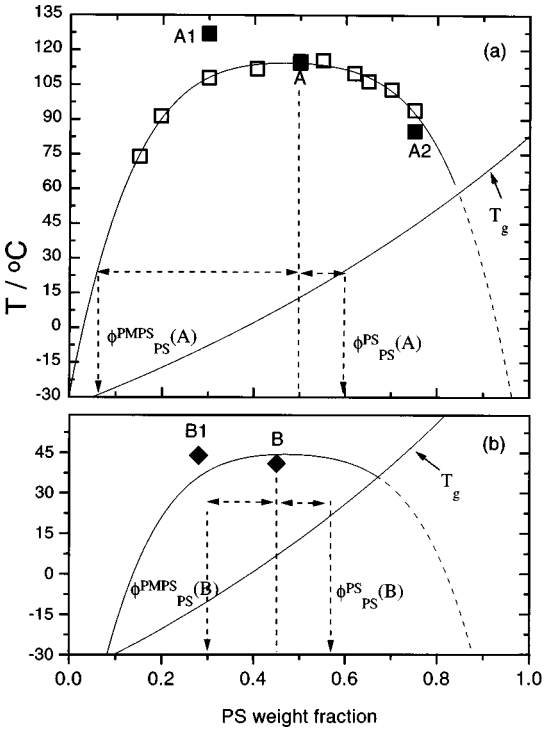

FIG. 2. Schematic representation of the phase diagram for A1, A, A2 (a) and B1, B (b) polystyrene/poly(methylphenylsiloxane) blends with different proximity between macrophase separation temperature T_s and the lowest temperature where complete phase separation takes place [the intersection of the phase diagram with the blend's average $T_g(\phi)$]. □, experimentally determined cloud points (Ref. 23) for mixtures consisting of the homopolymers of A. The spinodal decomposition of the initial concentration ϕ into mobile (PMPS-rich) and glassy (PS-rich) phases is indicated by the dashed arrows for blends A and B in (a) and (b), respectively. For all samples, a similar arrest of structure with nearly the same ϕ_{PS}, corresponding to ϕ, was observed. Solid symbols refer to the various blends at T_s; A-type (■) and B-type (◆); see also Table II.

III. RESULTS AND DISCUSSION

A. Phase diagram and glass transition scenario

Figure 2 depicts schematic representations of the phase diagrams of the various blends of Table II. The solid lines represent the binodal curves. For blends A, this curve has been determined experimentally, as described in Ref. 23, whereas for the other blends the corresponding curves are simply sketched based on the measured phase separation temperatures T_s which are also included in Fig. 2. The plotted concentration dependence of the $T_g(\phi)$ for these blends was estimated from the T_g's of the pure components. The temperatures T_s and $T_g(\phi)$ are relevant for the macrophase separation process of a blend with average composition ϕ. According to very recent 2D-computer simulations of a binary mixture undergoing a glass transition during phase separation[10] and earlier thermodynamic considerations,[17] the

decomposition process stops when $T \simeq T_g(\bar{\phi})$ while the domain morphology and composition should depend on the depth of the intersection between the $T_g(\phi)$ and the coexistence curve. Due to asymmetric phase separation the concentration distribution function $P(\phi)$ develops two maxima, from which only the one corresponding to the soft phase reaches the equilibrium concentration at the phase boundary. In contrast, the concentration field in the hard phase can strongly deviate from its local equilibrium affecting the composition and the volume fraction of this glassy phase. According to Ref. 17, the latter controls domain morphology and growth. Changes in the distribution function $P(\phi)$ in the critical region can also affect the largest scale motions, e.g., chain relaxation.[24]

The blends of Fig. 2, fall in two categories: Compositionally symmetric and asymmetric blends with large (samples A, A_1, and A_2) and small (samples B and B_1) difference between T_s and the lowest temperature T_i where complete phase separation takes place, according to the phase diagram [the latter is actually the temperature corresponding to the intersection of the blend's $T_g(\phi)$ with the binodal curve, as seen for example in Fig. 2]. The former blends (of the A-type), characterized by a wide temperature range for complete phase separation $T_s - T_i$, were found to exhibit a double peak structure in the dielectric $\epsilon''(\omega)$ spectra and a well defined morphological pattern [cf. Fig. 6(a)]; on the other hand, the latter blends (of the B-type), with a rather narrow temperature range for complete phase separation $T_s - T_i$, displayed a broad $\epsilon''(\omega)$ curve [cf. Sec. III D] and a smeared out composition field pattern [cf. Fig. 6(b)]. Information on the composition in the two phases will be extracted from the segmental dynamics in the phase separated blends.

B. Segmental dynamics and local environment

In order to facilitate the evaluation of the dynamic results, we summarize first the current view of the segmental dynamics in homogeneous blends. There is already strong experimental evidence of a two-step segmental relaxation in macroscopically disordered (single T_g) multiconstituent systems, e.g., blends and diblock copolymers with sufficiently large disparity in the T_g values between the two components, A and B (dynamic asymmetry).[3,4,6,7,13] A current theoretical account[9] is based on the hypothesis that segmental dynamics are determined by the effective local composition ϕ within a given ''cooperative'' volume $V(\phi)$. For a given average composition $\bar{\phi}$, the latter is not a constant but depends on ϕ, i.e., $V(\phi) = f(V_i, \phi)$ $(i = \mathrm{A,B})$. The component cooperative volume V_i is given by

$$V_i(\phi, T) = d_i^3 \left(\frac{T_0(\phi)}{T - T_0(\phi)} \right)^2, \tag{6}$$

where $T_0(\phi) = T_g(\phi) - c_2$, is the ideal glass transition temperature, d_i is a material characteristic length[9] and c_2 $(\simeq 50\ \mathrm{K})$ is the ideal WLF coefficient.

According to the thermodynamics of mixtures, the probability $P(\phi)$ for the occurrence of concentration fluctuations is symmetric around the mean $\bar{\phi}$, with variance $\langle |\Delta\phi|^2 \rangle = S(q)/V(\phi)$, where $S(q)$ is the static structure factor of the system. However, since the tessellation of space at a given T varies with the local ϕ, a bimodal probability density function can result from a large T_g contrast, thus rationalizing the presence of two distinct segmental relaxation processes in homogeneous polymer blends. As the hard component acquires larger cooperative volume [Eq. (6)] compared to the mobile component, the slow relaxation process corresponds mainly to the bulk average $\bar{\phi}$. Alternatively, the fast process relates to smaller cooperative volumes, rich in the mobile component. The deviation of this local composition ϕ from $\bar{\phi}$ and the disparity between fast and slow relaxation times in an athermal blend depends on the T_g contrast. In this view, the two phases of a heterogeneous system, may be described dynamically in a unified fashion, by envisaging each phase as a locally homogeneous region. Thus, the slow relaxation will provide an estimate of the average composition of this phase, whereas the fast process can give an estimate of the composition of the mobile component[9] due to the different reference volumes. On this basis, we proceed with the qualitative and quantitative account for the two classes of mixtures, characterized by distinctly different relative distances of the phase separation temperature from the lowest temperature characterized by complete phase separation, as mentioned earlier.

C. Wide temperature range of complete phase separation

Figure 3(a) depicts the dielectric loss factor (ϵ'') vs frequency for blend A over the temperature range where the pure PMPS component exhibits similar segmental dynamics. Similar results were obtained with blends A1 and A2 as well. The inset of Fig. 3(a) shows the normalized dielectric loss spectra ($\epsilon''/\epsilon''_{\max}$ vs $f/f_{\max}$) for blends A, A1, and A2, along with the spectrum of the PMPS homopolymer ($N = 20$, in Table I) at $T = 253$ K. It is apparent, that for these systems the observed dielectric loss corresponds to a PMPS-rich environment, since both relaxation time and relaxation shape are quite similar to those of the pure PMPS; the spectra of the blends are slightly broader. Since these spectra were reproducible over a period of a few weeks, we are justified to assume that the composition field in the mobile phase is stable within this time. The proximity of the fast and the pure PMPS relaxation times suggests that in this PMPS-rich phase, $\phi_1^1 \approx 1$. This volume fraction of the mobile PMPS-rich phase-1 can be estimated from the dielectric strength $\Delta\epsilon$ of the loss $\epsilon''(\omega)$ curves in the two phase regime. In general, in the case of macrophase separated binary polymer blends, the strength $\Delta\epsilon$ corresponding to the ith phase $(i = 1,2)$ can be expressed [Eq. (3)] by

$$\Delta\epsilon^{(i)} = \frac{N_A \rho}{3 k_B T} F \sum_{j=1,2} \frac{(\mu_j)^2 \lambda_j^i}{m_j} = \frac{N_A \rho w^{(i)}}{3 k_B T} F \sum_{j=1,2} \frac{(\mu_j)^2 \phi_j^i}{m_j}, \tag{7}$$

where λ_j^i is the fraction of the total jth segments $(j = 1,2)$ in the ith phase, $w^{(i)}$ is the mass fraction of the mixture in the

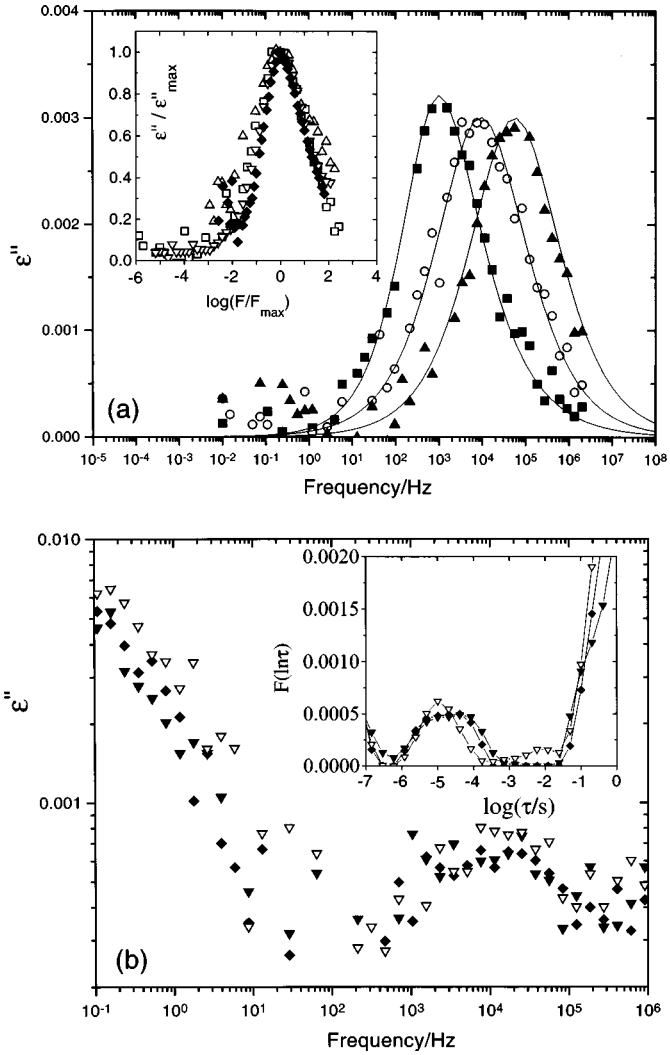

FIG. 3. (a) Dielectric loss spectra for the main fast process in blend A. At 248 K (■), 253 K (○), and 258 K (▲). The solid lines indicate HN fits [Eq. (4)] and the inset shows normalized spectra of the A1 (▽), A (□), and A2 (△) compared to that of bulk PMPS (◆). (b) $\epsilon''(\omega)$ for blend A at 298 K (▼), 303 K (◆), and 308 K (▽) along with the corresponding distribution relaxation functions $F(\ln \tau)$ [Eq. (5)] shown in the inset.

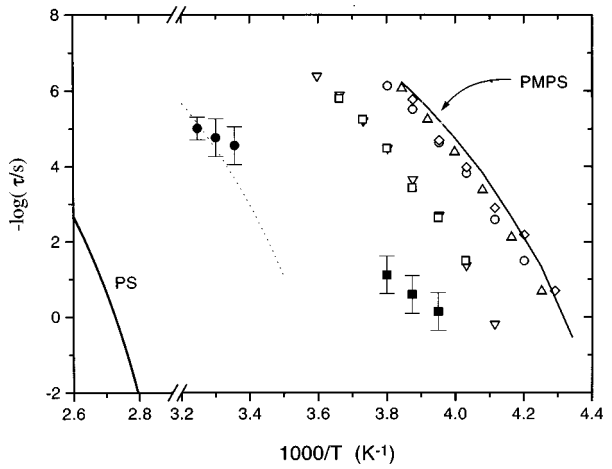

FIG. 4. Arrhenius temperature plot of the relaxation rates for the fast process (○, △, ◇: A, A1 and A2, ▽, □: B1, B blends) slow process (●: A, ■: B) and the single process in the constituent homopolymers (solid lines). The dotted line represents computed relaxation rates for an hypothetically homogeneous A blend. The data of the fast process were shifted to scale to the same PMPS T_g (as reference the blend A was used). Error bars in the rates of the slow processes are also shown.

ith phase, and ϕ_j^i the composition of the jth component in the ith phase. In the mobile rich in PMPS phase, we can ignore the contribution of PS in the expression of $\Delta\epsilon$ admitting an error of about 1%.[24] Further, according to the lever rule $w^{(1)}=(\phi_2^2-\bar{\phi})/(\phi_2^2-\phi_2^1)$ and hence $\Delta\epsilon_1^{(1)}$ relatively to the amplitude $\Delta\epsilon_1^{(0)}$ of the pure PMPS homopolymer can be written as

$$\Delta\epsilon_1^{(1)}/\Delta\epsilon_1^0=\lambda_1^1=w^{(1)}(1-\phi_2^1). \tag{8}$$

In Eq. (8) both ϕ_2^2 and ϕ_2^1 are, in principle, unknown. However, due to the proximity of the relaxation times in this mobile phase and bulk PMPS, ϕ_2^1 should be less than 0.1, implying a quite pure mobile phase (Fig. 2) in agreement with the 2D simulation result.[10] Then the value of ϕ_2^2 and the $T_g(\phi)$ curve can lead to a nominal temperature where the partitioning of the material into the two phases has taken place.

This procedure was applied to the blends A, and A_2 for which the phase diagram is experimentally available.[23] From the experimental $\Delta\epsilon$ between 248 and 258 K, λ_1^1 amounts to 0.17 and 0.06 for A and A2 blends, respectively. For the symmetric A blend, a variation of ϕ_2^1 in the interval [0, 0.1] corresponds to a nominal value of $\phi_2^2\simeq 0.6$ for the PS composition in the hard phase. As suggested by a visual inspection of the phase diagram of Fig. 2, the partitioning of the material at a temperature corresponding to the T_g of the PS-rich phase deviates significantly from its average local equilibrium value;[10] the separation process appears to cease as soon as the hard component's rich phase vitrifies,[10,13] in the current work approximately at $\phi_2^2\simeq\bar{\phi}$, i.e., at lower composition than that corresponding to T_i. The fraction of this phase $(1-w^{(1)})$ along with its concentration ϕ_1^2 in the dielectrically active PMPS suggests that a second slower process should be present in the experimental $\epsilon''(\omega)$ of blend A. In fact, a second $\epsilon''(\omega)$ peak is observed for the symmetric mixture A at high temperatures, as shown in Fig. 3(b), which is assigned to the PMPS segmental orientation in the PS-rich phase. The strength of this slow segmental relaxation, however, is about 20% less than expected, probably due to restricted orientational mobility of PMPS segments in the glassy phase. For the asymmetric A2 (rich in PS) blend, the lower fraction of the mobile phase is responsible for the weaker fast process compared to the A blend. Also the slow segmental process is not clearly resolved, as $\phi_2^2\simeq 0.8$ [Eq. (8)] and hence the PMPS composition in the hard phase is very small. An ultra slow process observed in the A and A2 (Fig. 7 below) is assigned to a Maxwell–Wagner polarization as will be discussed in Sec. III F.

The Arrhenius plot of Fig. 4 shows the relaxation times τ corresponding to the maximum of the distribution of relaxation times $F(\ln\tau)$ [Eq. (5)]. While the fast segmental process in A, A1, and A2 blends is almost as fast as pure PMPS, the characteristic times of the slow segmental process deviate sharply from either of the constituent homopolymers (solid lines in Fig. 4). Instead, the extracted slow relaxation times

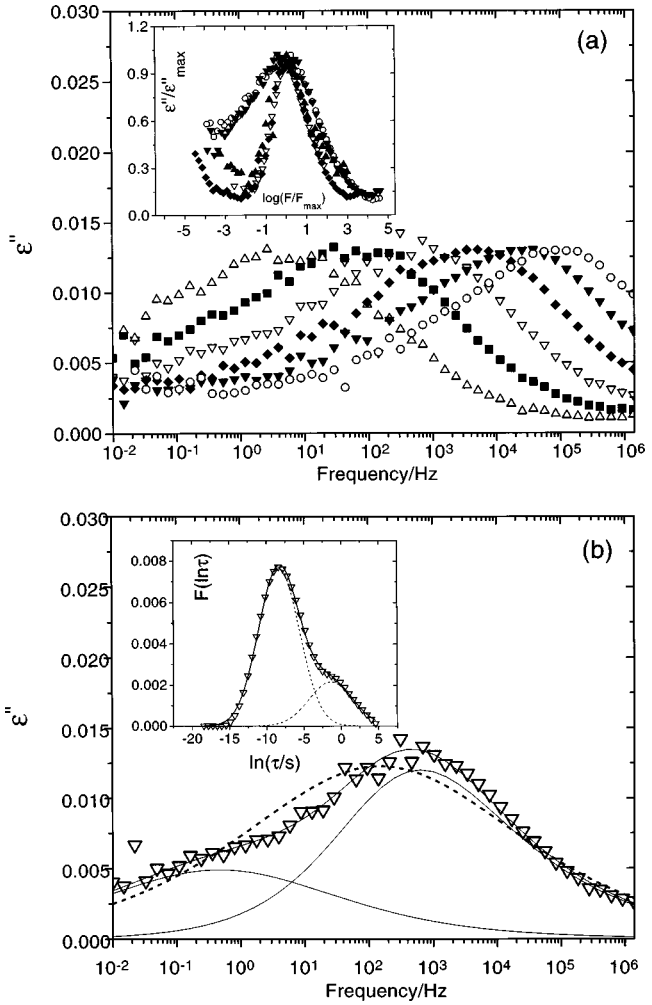

FIG. 5. (a) Dielectric loss spectra for blend B at 253 K (△), 258 K(■), 263 K (▽), 268 K (◆), 273 K, and 278 K (●). Inset: normalized $\epsilon''(\omega)$ for blend B1 (○) at 253 K, and B (▼) at 258 K compared to those of the three PMPS homopolymers of Table I (▲, ▽, ◆). (b) $\epsilon''(\omega)$ of blend B at 263 K represented by single (dashed line) or double (solid lines) HN functions [Eq. (4)], whereas the corresponding bimodal distribution relaxation function $F(\ln \tau)$ [Eq. (5)] is shown in the inset.

reside in the vicinity of a VFT temperature equation, $\log(\tau/\tau_0)=-B/(T-T_0)$, with composition-weighted average $T_0(\phi)$ and activation parameter B, in accordance with the composition of the hard phase.

D. Narrow temperature range of complete phase separation

For the blends B and B1 the separation temperature is located much closer to the intersection of the phase diagram of Fig. 2 and $T_g(\phi)$; the viscosity at T_s, is orders of magnitude higher in B than in A blend. The glass dynamics should therefore (Sec. III A) control spinodal decomposition, leading to an incomplete phase separation. The systems B were heated at temperatures higher than $T_{g,\mathrm{PS}}$ and allowed to reach the phase boundary by decreasing gradually the temperature; all measurements were reproducible within a time scale of several weeks. Typical dielectric loss spectra for blend B are depicted in Fig. 5, and a comparison with the $\epsilon''(\omega)$ of the PMPS homopolymer is shown in the normalized plot of the inset in Fig. 5(a), (Ref. 25), also including data for the B1 sample. The most striking feature of the data are the very broad shapes of the relaxation spectra extending over nearly 5 decades. Such an unexpected dynamic response strongly suggests an enhanced phase mixing, compared to a phase separated blend (Fig. 3, sec. III C). In addition, the shape of $\epsilon''(\omega)$ is asymmetric towards low frequencies as it is evident in the corresponding distribution of relaxation times [inset of Fig. 5(b)]; a ''shoulder'' systematically appears at long times. This notion is also corroborated by the fact that a satisfactory representation of the $\epsilon''(\omega)$ spectra requires a double HN function [Eq. (4)] process, as clearly shown in Fig. 5(b).

The relaxation times of the two processes are plotted in the transition map in Fig. 4. As illustrated in this plot, the faster process is nearly two decades slower compared to the respective PMPS homopolymer, whereas its adjacent slower one, is faster than the prediction of the VFT equation corresponding to the bulk average ϕ. Both processes are associated to the PMPS-rich phase and can be identified as the fast and the slow segmental mode anticipated from a homogeneous environment of the same composition (see below). In order to account for the content of the two components in this phase, one should take into consideration the presence of PS, which not only significantly modifies the local dynamics, but also has a small contribution to the observed dielectric spectrum, as inferred by the calculation of the associated dielectric strength. An estimation of $\Delta\epsilon$ of both processes in the temperature range 258–268 K (where the entire orientation relaxation function resides inside the experimental frequency window) presumes that more than 90% of the total intensity arises from this phase. In this context, a similar procedure as described in Sec. III C for blend A can be followed for the estimation of the local compositions, employing the lever rule in conjecture with

$$\Delta\epsilon^{(1)}=w_1[\phi_2^1\Delta\epsilon_{\mathrm{PS}}+(1-\phi_2^1)\Delta\epsilon_{\mathrm{PMPS}}], \tag{9}$$

which additionally accounts for the dielectric strength arising from the PS segments, due to incomplete phase separation.

In the case of blend B, the experimental phase diagram is not available, whereas the T_g's of the respective phases involve some ambiguity due to the broad transition, as shown in Fig. 1. Nevertheless, an estimation for the PS content in the PMPS-rich phase (ϕ_2^1), can be drawn, exploiting the argument that the dynamics of the slow segmental mode, should follow the average composition of the corresponding phase (Sec. III A). On this basis, ϕ_2^1 can be expressed[3] as

$$\varphi_2^1=\frac{B_2[B_1-\kappa_1(T-T_{01})]}{\kappa_1[B_1(T-T_{02})-B_2(T-T_{01})]}, \tag{10}$$

where T_{0i}, B_i represent the VFT parameters of the ith component, $\kappa_1=\log\tau-\log\tau_0$ is computed from the experimental values of the segmental relaxation times in the region rich in component 1 (here PMPS), and $\tau_0=10^{-13}$ s. Equation (10) leads to $\phi_2^1\simeq 0.3$, while substitution of this value in Eq. (9) yields $\phi_2^2\simeq 0.57$. In consensus with the discussion for blend A in the previous section, this result manifests the recess of unmixing by virtue of the blend's T_g intervention,[13] taking

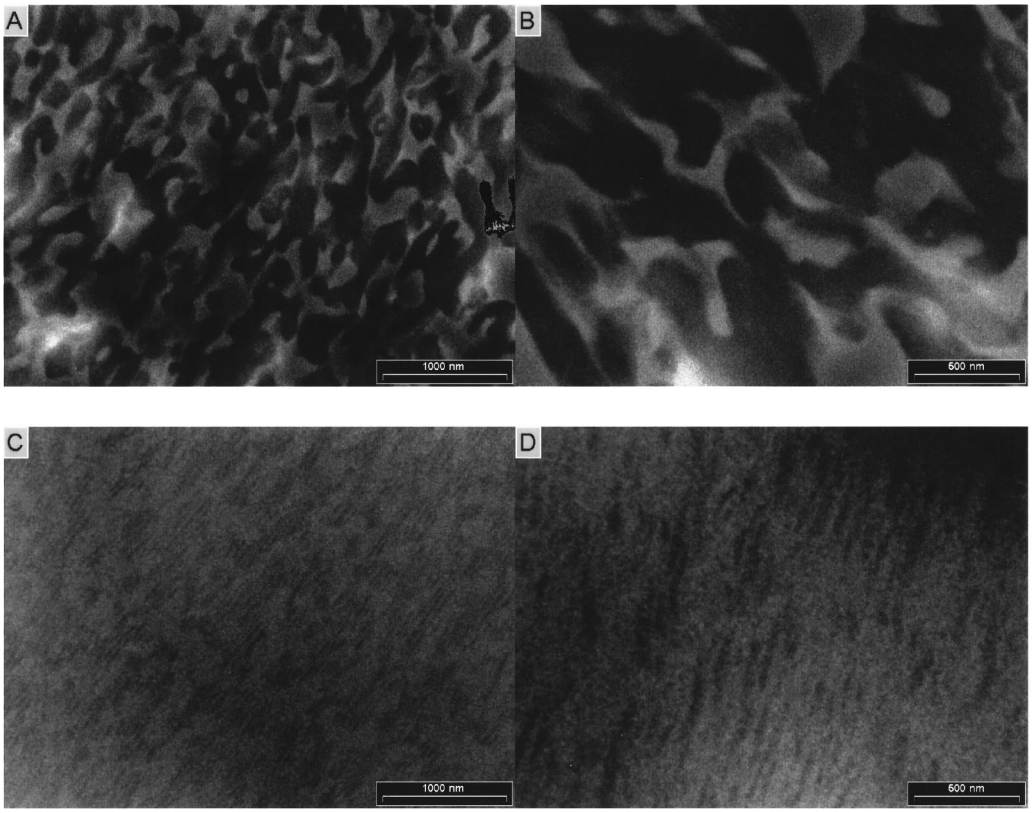

FIG. 6. Transition electron microscopy images for two blends in two magnifications: blend A1 (cases A, B) and blend B (cases C, D). Dark and bright areas represent the PS-rich and PMPS-rich regions, respectively.

place though in earlier stages, as evidenced by the proximity of the spinodal temperature to the glass transition [Fig. 2(b)], as discussed before.[26]

Considering now the PS-rich environment, a simple calculation (based on the computed local compositions) assumes that about 55% of the mixture is partioning in the hard phase with $\phi_1^2=0.43$ in PMPS. In fact, an indication of a third slower relaxation is present in the experimental $\epsilon''(\omega)$ at high temperatures (not shown here). Analogous dynamic behavior was displayed by the B1 blend. The third slow process should not be confused with the ultra slow process mentioned in Sec. III C for A blends, (Fig. 7 below); its presence in blends B is probably obscured due to the high conductivity contribution and/or weak amplitude (Sec. III F).

E. Morphological evidence

The striking difference in the two-phase state dynamic behavior of the blends (as classified earlier) has been attributed to the local environments resulting from the separation process. It is therefore necessary to confirm the dynamic findings with morphological studies. Figure 6 presents typical TEM images (in successive magnification) for blends A1 (cases A, B) and B (cases C, D). As is clearly seen, a two-phase structure characterized by well-separated regions of rich in either of the two polymers is formed in A1. In contrast, at the same magnification, blend B reveals a more diffused (mixed) interconnected pattern.

The growth process is clearly much more advanced in A1, as reflected in the domain size. For this sample, the volume fraction of the glassy phase is less than 0.5, and hence the mobile phase forms the percolating matrix allowing the coarsening of the domain pattern.[10] In this composition field [Fig. 6(a)] with large concentration contrast, the fast narrow $\epsilon''(\omega)$ peak [Fig. 3(a)] is associated with space regions almost pure in PMPS due to the rather short sampling volume $V(\phi)$ [Eq. (6)]. The second well-separated slow process [Fig. 3(b)] characterizes regions rich in PS but far from the local (thermodynamic) equilibrium value, as implied by the values of the relaxation rates; these are much faster than in almost pure PS-phase. Thus, the dark (PS) regions in Fig. 6(a) are not pure phases.

Blend B, on the other hand, displays significantly higher degree of mixing, as depicted in the TEM images of Fig. 6(b). This morphological picture is in accordance with the inhibited coarsening of the domain structure in B, compared to A (Fig. 2), and hence the low concentration contrast between separated regions. Since phase decomposition in Fig. 2(b) was obtained from local dynamics, with inherently larger magnification [of $O(\mathrm{nm})$] than the TEM image, these results moreover suggest that the domain pattern is statistically self-similar. Based on the current picture of segmental relaxation in two component systems (Sec. III B), the extended mixing in B can rationalize the broad bimodal of $\epsilon''(\omega)$ (Fig. 5) in the mobile phase, due to significant concentration fluctuations, whereas the (third) slower process is associated with the hard phase probed by larger $V(\phi)$ [Eq. (6)]. However, while segmental dynamics, being sensitive to small-scale spatial-heterogeneities, can provide information

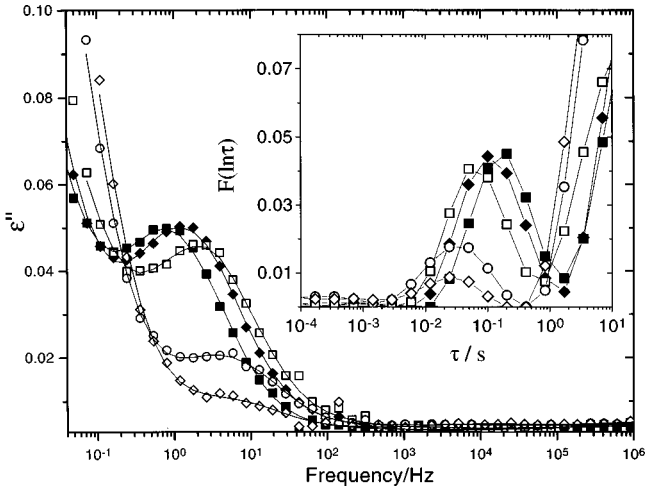

FIG. 7. Dielectric loss spectra of A2 blend at 323 K (■), 334 K (♦), 343 K (□), 358 K (○), and 363 K (◇) along with the corresponding distribution relaxation functions [Eq. (5)], shown in the inset.

on the local composition and volume fraction of each phase already at early stages of decomposition, the domain size cannot be inferred from these data; the coarsening of the domain morphology is probably manifested in the ultra slow process.[27] The different domain sizes in Fig. 6 might relate to the volume fraction of the hard phase in the two samples. In blend B, the latter forms the percolating matrix which can affect the coarsening mechanism. A detailed morphological study using different volume fractions of the hard component (PS) and comparison with the pertinent predictions of Ref. 10 is in progress.

F. The ultra slow relaxation process

In the context of the detailed dynamic description of the two-phase region with DS, valuable information relating to the morphology of the mixture in this regime can be extracted by analyzing the slower process, shown for example in Fig. 7 for the A2 blend. As evidenced from this figure, the slower process possesses significantly higher intensity, compared to either of the other modes, or even more to a nominally PS-rich phase. Further, it exhibits a very weak temperature dependence (Fig. 7) and loses intensity (more prominently in blend A2, since in blends A and B1 it interferes with conductivity) as the system approaches the homogeneous phase. This dielectric loss is identified with a Maxwell–Wagner polarization process,[20,27] usually observed in mixtures of materials with a high dielectric permittivity or conductivity contrast. The dielectric strength associated with such a process can acquire extremely high values, depending on the difference of the dielectric quantities of the constituent materials, as well as on the shape and extend of spatial heterogeneities of the system.[20] Several observations of the Maxwell–Wagner process have already been reported in the two-phase region of polymer blends,[28] conforming to the large scale of local heterogeneities in such systems. In the case of a binary mixture consisting of a continuous matrix and a homogeneously dispersed phase, with frequency-independent permittivity and conductivity, it is observable as a Debye-type relaxation with weak (if any) temperature dependence of the maximum of the loss peak. The characteristic frequency of such a process is given by[20]

$$f_{\mathrm{MW}}=\frac{(1-n)\sigma_m+n\sigma_i+n\phi(\sigma_m-\sigma_i)}{2\pi\epsilon_0[(1-n)\epsilon_m+n\epsilon_i+n(\epsilon_m-\epsilon_i)]}, \tag{11}$$

where ϵ is the dielectric constant, σ the conductivity and ϕ the volume fraction of the minority phase. The subscripts i,m stand for inclusion and matrix, respectively, while n is a shape factor describing the geometry of the inclusions: for spheres: $n=1/3$, prolate spheroids: $n\leqslant 1/3$, and oblate spheroids: $1/3\leqslant n\leqslant 1$.

The above equation which is valid for small ϕ (so that the inclusion-matrix assumption is preserved), has been extensively applied with success in systems of this type.[29] For cases of higher ϕ, special techniques (e.g., asymmetric integration) have been developed to tackle this situation. In our case, the matrix-inclusion type of dispersion is consistent with the anticipated morphology of the two equilibrium phase-separated (according to their spectra, as discussed before) asymmetric blends A1 and A2. Based on the above information, we can compare the predictions of this model with our measurements for the blend A2. Although the dielectric constants of PS and PMPS homopolymers are very close, conductivity measurements in these systems resulted in a difference of nearly two orders of magnitude, namely $\sigma_{\mathrm{PS7600}}\simeq 1.9\times 10^{-15}$ $(\Omega\ \mathrm{cm})^{-1}$ and $\sigma_{\mathrm{PMPS2724}}\sim 4.4\times 10^{-13}$ $(\Omega\ \mathrm{cm})^{-1}$ at a frequency of 1 Hz. Application of Eq. (11), assuming spherical inclusions with volume fractions of $\phi=0.1$ and $\phi=0.2$, predicts for the characteristic frequency of the Maxwell–Wagner process $f_{\mathrm{MW}}\simeq 7.5\times 10^{-2}$ Hz, and $f_{\mathrm{MW}}\simeq 6.5\times 10^{-2}$ Hz, respectively. Furthermore, a variation of the shape factor (for instance for $\phi=0.2$) from 0.1 to 0.9 (and thus including the case of asymmetric inclusions as suggested from the TEM images of blend A1) results in a change of the predicted frequency between 2×10^{-2} Hz and 2.5×10^{-1} Hz, in relatively good agreement with experimental observations.

IV. CONCLUSIONS

In this study we have presented a systematic dynamic characterization of the phase separated regime, in a series of binary polymer blends, PS/PMPS with large T_g contrast between the components, by examining the dynamic behavior of the two phases on a segmental level by dielectric spectroscopy. The cessation of unmixing, due to the intervention of the glass transition temperature, as suggested in an earlier study[13] and recent simulations,[10] was clearly demonstrated, while the existence of distinct local environments, depending on the distance between mixture's separation temperature and the hard phases' T_g, was verified by TEM morphological studies. Moreover, a quantitative description in terms of local composition in each phase was possible, rendering thus DS a useful tool for mapping the dynamic phase state of such systems.

ACKNOWLEDGMENTS

This work was partially supported by the E.U. (Brite/Euram program, Contract No. BRE2-CT94.0610; Ultraviolet Laser Facility at FORTH-IESL, under the Large Installations Plan). We are thankful to Th. Wagner for the preparation of the polymers. G.M. appreciates the warm hospitality of FORTH.

[1] X. Quan, G. Johnson, E. Anderson, and F. Bates, Macromolecules **22**, 2451 (1989); X. Quan, G. Johnson, E. Anderson, and H. Lee, *ibid.* **24**, 6500 (1991).
[2] C. Roland and K. Ngai, Macromolecules **24**, 2661 (1991); **28**, 4033 (1995).
[3] G. Fytas, S. H. Anastasiadis, K. Karatasos, and N. Hadjichristidis, Phys. Scr. **49**, 237 (1993).
[4] A. Alegria, J. Colmenero, K. Ngai, and C. Roland, J. Chem. Phys. **98**, 7588 (1993); A. Alegria, C. Elizextea, I. Cendoya, and J. Colmenero, Macromolecules **28**, 8819 (1995); A. Alvarez, A. Alegria, and J. Colmenero, *ibid.* **27**, 4486 (1994).
[5] A. Zetsche and E. Fischer, Acta Polym. **45**, 168 (1994).
[6] G. Chung, J. Kornfield, and S. Smith, Macromolecules **27**, 964,5729 (1994); B. Arendt, R. Kannan, M. Zewail, J. Kornfield, and J. Smith, Rheol. Acta **27**, 964 (1994).
[7] G. Fytas, G. Meier, and D. Richter, J. Chem. Phys. **105**, 1208 (1996); K. Karatasos, G. Fytas, S. Kumar, G. Floudas, and J. Roovers (in preparation).
[8] A. Khokhlov and I. Erukhimovic, Macromolecules **26**, 7195 (1993); P. Kahlatur, A. Khokhlov, and V. Vasilevskaya, Macromol. Theory Simul. **3**, 939 (1994).
[9] S. Kumar, R. Colby, S. H. Anastasiadis, and G. Fytas, J. Chem. Phys. **105**, 3777 (1996).
[10] D. Sappelt and J. Jäckle, Europhys. Lett. **37**, 13 (1997); Physica A **240**, 453 (1997).
[11] H. Tanaka, J. Chem. Phys. **105**, 10099 (1996); Phys. Rev. Lett. **76**, 787 (1996).
[12] T. Taniguchi and A. Onuki, Phys. Rev. Lett. **77**, 4910 (1996).
[13] G. Meier, D. Vlassopoulos, and G. Fytas, Europhys. Lett. **30**, 325 (1995).
[14] T. W. Smith, M. A. Abramowitz, G. C. Conway, D. J. Luca, J. M. Serpico, and G. E. Wnek, Macromolecules **29**, 5042 (1996).
[15] H. Takeno, S. Koizumi, H. Hasegawa, and T. Hashimoto, Macromolecules **29**, 2440 (1996).
[16] A. Zetsche, K. Kremer, and W. Jung, Polymer **31**, 1883 (1990); H. Yang, S. Ricci, and M. Collins, Macromolecules **24**, 5218 (1991).
[17] F. Frank and A. Keller, Polym. Commun. **29**, 186 (1988).
[18] L. Reimer, in *Advances in Electronics and Electron Physics*, edited by P. W. Hawkes (Academic, New York, 1991), Vol. 81; A. Du Chesne, G. Lieser, and G. Wegner, Colloid Polym. Sci. **272**, 1329 (1994); A. Du Chesne, K. Wenke, G. Lieser, and G. Wenz, Acta Polym. **48**, 142 (1997).
[19] K. Adachi, Y. Imanishi, and T. Kotaka, J. Chem. Soc. Faraday Trans. **85**, 1083 (1989); G. Fytas, I. Alig, A. Rizos, and F. Kremer, Polymer **34**, 2263 (1993); I. Alig, F. Kremer, G. Fytas, and J. Roovers, Macromolecules **25**, 5277 (1992); J. Kanetakis, G. Fytas, F. Kremer, and T. Pakula, *ibid.* **25**, 3484 (1992).
[20] G. Williams, Chem. Soc. Rev. **7**, 89 (1978); Adv. Polym. Sci. **39**, 59 (1979); Chem. Rev. **72**, 55 (1972); H. Fröhlich, *Theory of Dielectrics* (Clarendon, Oxford, 1958); G. Williams, Adv. Polym. Sci. **39**, 59 (1979); B. Scaife, *Principles of Dielectrics* (Oxford, New York, 1989); L. Van Beek, *Progress in Dielectrics*, edited by J. B. Birks (Heywood, London, 1967), Vol. 7.
[21] S. Havriliak, and S. Negami, J. Polym. Sci. C **14**, 99 (1966); S. Havriliak and S. Negami, Polymer **8**, 161 (1967).
[22] K. Karatasos, S. H. Anastasiadis, A. N. Semenov, G. Fytas, M. Pitsikalis, and N. Hadjichristidis, Macromolecules **27**, 3459 (1994); F. Alvarez, A. Alegria, and J. Colmenero, J. Chem. Phys. **103**, 1 (1995).
[23] D. Vlassopoulos, A. Koumoutsakos, S. H. Anastasiadis, S. Hatzikiriakos, and P. Englezos, J. Rheol. **41**, 739 (1997).
[24] A. K. Rizos, G. Fytas, and A. N. Semenov, J. Chem. Phys. **102**, 6935 (1995). This error was estimated as $\Delta(\Delta\epsilon_1)/\Delta\epsilon_1 < (\mu_2/\mu_1)^2\ (m_1/m_2)\ (1-\phi_1^1)$ with $\mu_1 = 0.69$ D, $\mu_2 = 0.20$, and $\phi_1^1 \simeq 0.9$.
[25] Note that, we compare $\epsilon''(\omega)$ recorded at different temperatures, since over the examined range their shape remains virtually constant.
[26] The composition of PS in the PMPS-rich phase (0.3) apparently deviates from that corresponding to the intersection with the sketched phase boundary in Fig. 2(b) (about 0.22); this is probably due to the fact that we do not know the phase diagram of *B*-type blends, as already discussed in the text, and the sketch is only indicative of the phase behavior (the main point is the intersection of glass transition).
[27] J. A. Maxwell *A Treatise on Electricity and Magnetism* (Oxford University Press, Oxford, 1892); K. Wagner, *Isolierstoffe der Elektrotechnik* (Springer, Berlin, 1924).
[28] R. Welton, W. MacKnight, J. Fried, and F. Karasz, Macromolecules **11**, 158 (1978); M. Dionisio, J. Ramos, and A. Fernandes, in *Proceedings of the Fifth European Symposium on Polymer Blends*, pp. 243–244 (1996); D. Hayward, R. Pethrick, and T. Siriwittayahorn, Macromolecules **25**, 1480 (1992).
[29] P. Aldrich, R. McGee, S. Yalvac, J. Bonekamp, and S. Thurow, J. Appl. Phys. **62**, 4504 (1987); A. North and J. Reid, Eur. Polym. J. **8**, 1129 (1972); G. Perrier and A. Bergeret, J. Appl. Phys. **77**, 2651 (1995).